nature physics

SUPPLEMENTARY INFORMATION

DOI: 10.1038/NPHYS3905

Ultrastrong coupling of a single artificial atom to an electromagnetic continuum in the nonperturbative regime

P. Forn-Díaz,[1] J. J. García-Ripoll,[2] B. Peropadre,[3] J.-L. Orgiazzi,[4] M. A. Yurtalan,[4] R. Belyansky,[4] C. M. Wilson,[4] and A. Lupascu[1]

[1]*Institute for Quantum Computing, Department of Physics and Astronomy, and Waterloo Institute for Nanotechnology, University of Waterloo, Waterloo, N2L 3G1, Canada*

[2]*Instituto de Física Fundamental IFF-CSIC, Madrid 28006, Spain*

[3]*Department of Chemistry and Chemical Biology, Harvard University, Cambridge, Massachusetts 02138, United States*

[4]*Institute for Quantum Computing and Department of Electrical and Computer Engineering, University of Waterloo, Waterloo, N2L 3G1, Canada*

S0: MEASUREMENT SETUP

Experiments on the device in Fig. 2(a) of the main text and the tunable device were performed in a dilution refrigerator with a base temperature of 9 mK where the chip is thermally anchored to. Our wiring is configured to measure both in reflection as well as in transmission using different input ports, although in this work we only show the transmission measurements. The optimal measurement bandwidth of the system is 4-8 GHz. The on-chip transmission line is followed by two circulators behind a cryogenic amplifier (see Fig. 1 for the full circuit diagram) anchored at 3.2 K with noise temperature of ~ 5 K. We further amplify the signals at room temperature and digitize them using either a vector network analyzer or a spectrum analyzer. The device in Fig. 2(b) of the main text was characterized in a different dilution refrigerator with a base temperature of 15 mK, and having a similar wiring configuration as the one shown in Fig. 1 except for a larger nominal measurement bandwidth of 3-11 GHz.

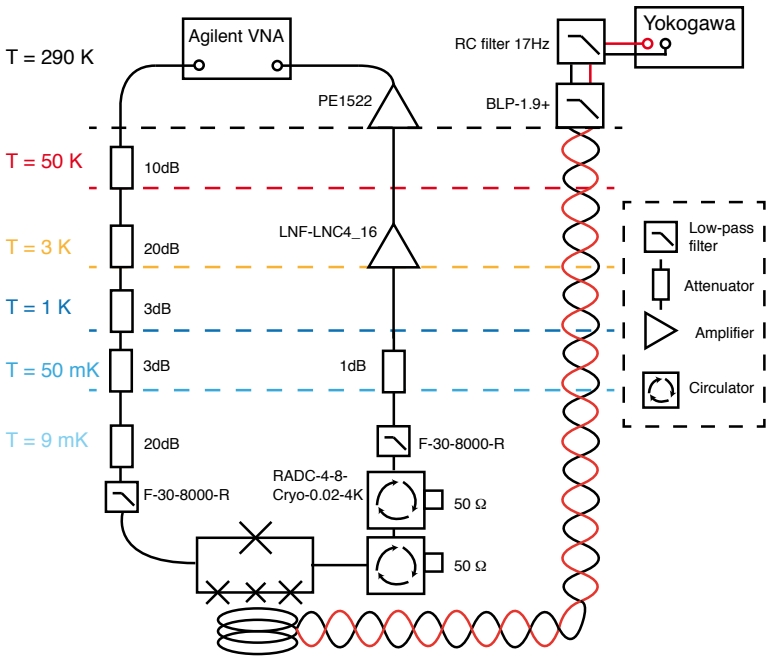

FIG. 1. Schematic of the full circuit for transmission measurements.

S1: QUBIT HAMILTONIAN AND TUNABLE COUPLING OPERATOR

The circuit layout of a flux qubit galvanically tunably coupled to a transmission line with a SQUID-loop shared between the two can be seen in Fig. 2.

The Lagrangian of the qubit can be written down by considering the fluxoid quantization condition on the separate

DOI: 10.1038/NPHYS3905

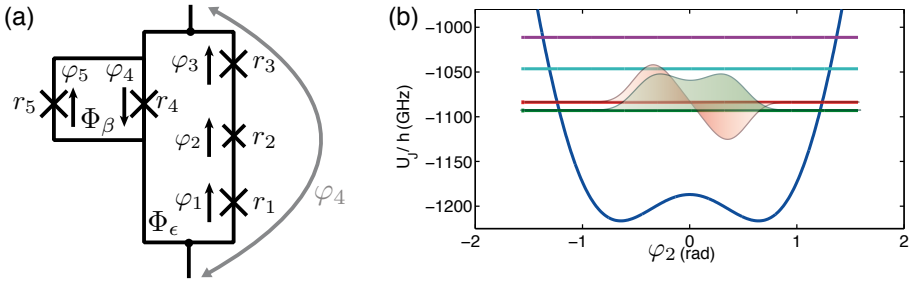

FIG. 2. (a) Schematic of the circuit layout of a flux qubit sharing a SQUID-junction with a transmission line. The coefficients r_1, r_2, r_3, r_4, r_5 represent the size of the junctions. For the device used in the experiment, $r_2 = 0.62, r_4 = 2.6, r_1 = r_3 = r_5 = 1$. (b) Qubit potential with first four energy levels for $\Phi_\beta = 0$, $\Phi_\epsilon = \Phi_0/2$ together with the wave functions of the lowest two levels for the ground (symmetric) and first excited state (antisymmetric). The parameters used are similar to the device with tunable coupling of the main text, $E_J/E_C \simeq 70, E_J/h \simeq 350$ GHz. Notice that the levels lie above the barrier as is usual for flux qubits with level splittings in the GHz range [1].

loops:

$$\varphi_1 + \varphi_2 + \varphi_3 + \varphi_4 + 2\pi f_\epsilon = 0, \tag{1}$$
$$\varphi_4 + \varphi_5 + 2\pi f_\beta = 0, \tag{2}$$

where $f_\epsilon = \Phi_\epsilon/\Phi_0$, $f_\beta = \Phi_\beta/\Phi_0$ are the magnetic frustration in each loop. Using $\varphi_1, \varphi_2, \varphi_4$ as the independent degrees of freedom, the Lagrangian of the qubit reads [2]:

$$\mathcal{L}(\varphi_1,\varphi_2,\varphi_4,\dot\varphi_1,\dot\varphi_2,\dot\varphi_4) = \frac{\varphi_0^2 C}{2}\left(r_1\dot\varphi_1{}^2 + r_2\dot\varphi_2{}^2 + (r_4+r_5)\dot\varphi_4{}^2 + r_3(\dot\varphi_1+\dot\varphi_2+\dot\varphi_4)^2\right) + E_J\left(r_1\cos\varphi_1 + r_2\cos\varphi_2 + r_4\cos\varphi_4 + r_3\cos(-2\pi f_\epsilon - \varphi_1 - \varphi_2 - \varphi_4) + r_5\cos(-2\pi f_\beta - \varphi_4)\right). \tag{3}$$

Here we defined the reduced flux quantum $\varphi_0 = \Phi_0/2\pi$, C is the capacitance of junction with size $r = 1$, $E_J = I_C\varphi_0$. The canonical momenta $q_i = \partial\mathcal{L}/\partial\dot\varphi_i$ are related to the derivative of the conjugate phase operator:

$$\begin{pmatrix}\dot\varphi_1\\ \dot\varphi_2\\ \dot\varphi_4\end{pmatrix} = \frac{1}{C\varphi_0^2}\frac{1}{\det(K)}\begin{pmatrix} r_3(r_4+r_5)+r_2(r_3+r_4+r_5) & -r_3(r_4+r_5) & -r_3r_2\\ -r_3(r_4+r_5) & r_3(r_4+r_5)+r_1(r_3+r_4+r_5) & -r_3r_1\\ -r_3r_2 & -r_3r_1 & r_2r_3+r_1(r_2+r_3)\end{pmatrix}\begin{pmatrix}q_1\\ q_2\\ q_4\end{pmatrix}, \tag{4}$$

where $\det(K) = r_2r_3(r_4+r_5) + r_1(r_3(r_4+r_5) + r_2(r_3+r_4+r_5))$ is the dimensionless determinant of the capacitance matrix. We can now write down the Hamiltonian following a Legendre transformation $\mathcal{H} = \sum_i q_i\dot\varphi_i - \mathcal{L}$:

$$\mathcal{H} = \frac{4E_C}{r_2r_3(r_4+r_5)+r_1(r_3(r_4+r_5)+r_2(r_3+r_4+r_5))}\left(n_1^2(r_3(r_4+r_5)+r_2(r_3+r_4+r_5)) + n_2^2(r_3(r_4+r_5)+r_1(r_3+r_4+r_5)) + n_4^2(r_2r_3+r_1(r_2+r_3)) - 2n_1n_2r_3(r_4+r_5) - 2n_4r_3(r_1n_2+r_2n_1)\right) - E_J\left(r_1\cos\varphi_1 + r_2\cos\varphi_2 + r_4\cos\varphi_4 + r_3\cos(-2\pi f_\epsilon - \varphi_1 - \varphi_2 - \varphi_4) + r_5\cos(-2\pi f_\beta - \varphi_4)\right). \tag{5}$$

Here we defined the quantized charge operator $n_i = \hbar q_i$ as well as the charging energy $E_C = e^2/2C$. If we set $f_\beta = 0$ the last term in the Josephson energy becomes $r_5\cos\varphi_4$, which combined with the r_4 term becomes an effective junction of size $(r_4 + r_5)$. For $f_\beta = 0.5$, the last term becomes $-r_5\cos\varphi_4$, which now leads to an effective junction of size $(r_4 - r_5)$. Therefore we can tune the effective size of the coupling junction without affecting much of the rest of the qubit Hamiltonian. The different junction size will unavoidably lead to modifications of the qubit splitting.

In order to diagonalize the Hamiltonian it is convenient to find its representation in the charge basis $\{|n\rangle\}$ where the Josephson terms have a simple expression, since [2]

$$\cos\varphi|n\rangle = \frac{e^{i\varphi}+e^{-i\varphi}}{2}|n\rangle = \frac{|n-1\rangle + |n+1\rangle}{2}. \tag{6}$$

The Josephson terms are therefore not represented by a closed Hilbert subspace in the charge basis. Therefore we need to restrict the number of charges between $-n_{\max}$ and $n_{\max}$ for each degree of freedom. Usually for $n_{\max} = 10$ the error in the eigenenergies is less than 1%. Fig 2(b) shows the calculated qubit energies and wavefunctions for $f_\beta = 0$ and $f_\epsilon = 0.5$ using $n_{\max} = 10$.

S1.1: Energy levels and Crosstalk

For a given set of fluxes (f_ϵ, f_β) we can find the eigenenergies and eigenstates of the qubit. For all calculations shown in this section we take the values close to the experiment with the tunable coupling device $r_1 = r_3 = 1.0, r_2 =$

$0.6, r_4 = 1.0, r_5 = 2.6$, $E_J/E_C = 70$, $E_J/h = 300$ GHz, $n_{\max} = 10$. The areas of the two qubit loops are seen to be $A_\epsilon/A_\beta \simeq 8.3$, which agree with the data as seen in the calculations of Fig. 4(b) of the main text. In order to reproduce the experimental spectra we sweep the flux in the ϵ-loop and assume the flux in the beta loop to be proportional to it, $\Phi_\beta = \Phi_\epsilon/8.3$.

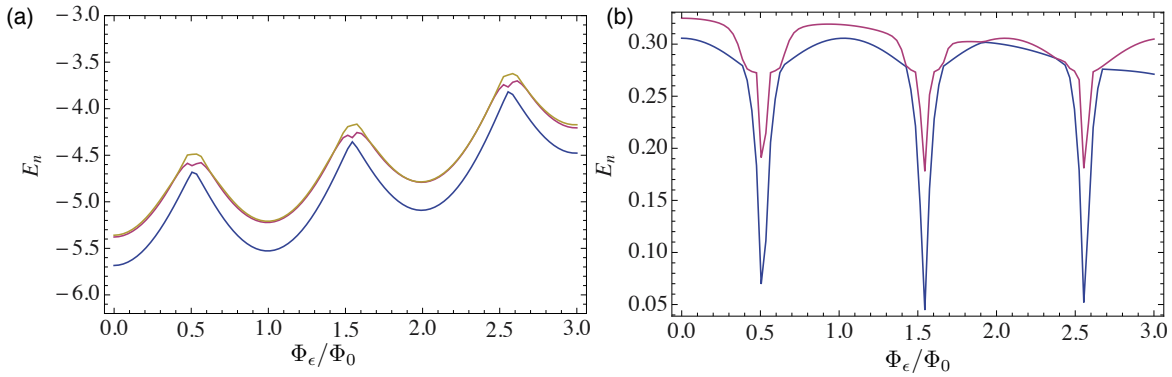

FIG. 3. (a) Calculated three lowest energy levels of the Hamiltonian in Eq (5) as function of Φ_ϵ taking into account that $\Phi_\beta = \Phi_\epsilon/8.3$. The energies are in units of E_J. (b) Energy differences with respect to the ground state energy. Notice that qubit symmetry points are not falling on top of $\Phi/\Phi_0 = 0.5$ due to the interference between the two qubit loops.

The resulting spectra in Fig. 3 clearly show a lack of periodicity, as would be expected for a qubit with no SQUID-loop. The qubit symmetry points do not agree with $\Phi_\epsilon = \Phi_0(1/2 + n)$, n being an integer. The difference is due to the interference between the two qubit loops. The potential energy terms related to the applied fluxes are

$$r_4 \cos(-2\pi f_\epsilon - \varphi_1 - \varphi_2 - \varphi_3) + r_5 \cos(-2\pi(f_\beta + f_\epsilon) - \varphi_1 - \varphi_2 - \varphi_3). \tag{7}$$

In analogy with the usual flux qubit potential [3], we can rewrite these terms as an effective new Josephson term $\tilde{U}$ with effective critical current $\tilde{I}$ and effective flux $\tilde{f}$ as $\tilde{U}/E_J = -\tilde{I}\cos(-\varphi_1 - \varphi_2 - \varphi_4 + 2\pi\tilde{f})$. Expanding the cosine terms, we can relate $\tilde{f}$ and $\tilde{I}$ with the rest of parameters:

$$-\tilde{U}/E_J = \tilde{I}(\cos\varphi_\Sigma \cos 2\pi\tilde{f} - \sin\varphi_\Sigma \sin 2\pi\tilde{f}), \tag{8}$$

$$= \cos\varphi_\Sigma(r_4 \cos 2\pi f_\epsilon + r_5 \cos(2\pi(f_\epsilon + f_\beta)) - \sin\varphi_\Sigma(r_4 \sin 2\pi f_\epsilon + r_5 \sin 2\pi(f_\epsilon + f_\beta)), \tag{9}$$

where $\varphi_\Sigma = \varphi_1 + \varphi_2 + \varphi_3$. In particular, at the symmetry point $\tilde{f} = 1/2$ which cancels the second term in Eq. (8). This implies that the term multiplying $\sin\varphi_\Sigma$ has to be zero, leading to a transcendental equation to obtain the location of all symmetry points:

$$-\frac{r_4}{r_5} = \frac{\sin 2\pi f_\epsilon}{\sin 2\pi(f_\epsilon + f_\beta)}. \tag{10}$$

In addition to equation (10) we also impose the condition $\cos(2\pi\tilde{f}) = -1$, that is

$$-1 = r_4 \cos 2\pi f_\epsilon + r_5 \cos 2\pi(f_\epsilon + f_\beta). \tag{11}$$

We calculate the difference between consecutive qubit symmetry points in Fig. 4(a) over a period of Φ_β. The cosine-like modulation clearly shows the interference between the two loops. The experimentally measured difference in periodicity of the qubit symmetry points is plotted in Fig. 4(b). A modulation of the periodicity is also clear. The relative change of periodicity of $\sim 10\%$ agrees with the prediction of Eqs. (10), (11). Fig. 4(b) is scaled to the value at $\Phi_\beta/\Phi_0 = 0$. Fig. 4(a) is scaled such that "1" in the vertical axis would correspond to $\Phi_\epsilon/\Phi_0 = 0.5$.

The qubit Lagrangian shown here does not include geometric capacitance between islands and to ground. We have inspected the effect of those terms and found less than 10% variation in the qubit frequency.

S1.2: Coupling operator

As shown in Ref. [4], the coupling strength of a flux qubit sharing a junction with a resonator or a transmission line is given by the modulus of the matrix element of the phase operator across the coupling junction $|\langle 1|\hat{\varphi}_i|0\rangle|$. In the circuit of Fig. 2 this corresponds to the phase across $\hat{\varphi}_4$. The coupling operator can be expressed in the qubit basis states using that the representation in the charge basis of the phase operator is

$$\langle n|\hat{\varphi}|m\rangle = \frac{1}{2\pi}\int_{-\pi}^{\pi} \hat{\varphi} e^{-i(m-n)\hat{\varphi}} \mathrm{d}\hat{\varphi} = \begin{cases} 0 & \text{if } m = n, \\ -i\frac{(-1)^{(m-n)}}{m-n} & \text{if } m \neq n. \end{cases} \tag{12}$$

DOI: 10.1038/NPHYS3905

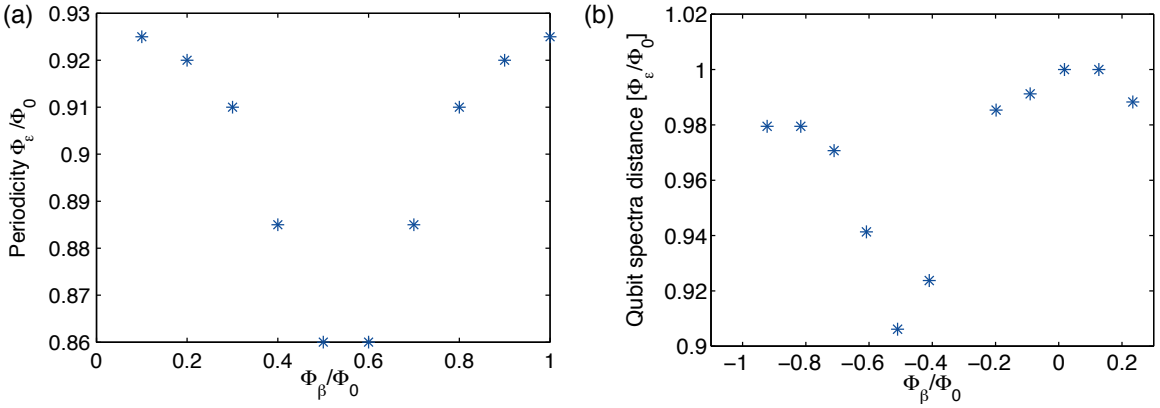

FIG. 4. (a) Calculated difference in consecutive qubit symmetry points as function of flux in ϵ-loop, using Eqs. (10), (11). (b) Experimentally measured distance between qubit periods. The relative change of period $\sim 10\%$ for both plots (a) and (b) agrees quite well. The difference in (b) at $\Phi_\beta/\Phi_0 = 0$ and $\Phi_\beta/\Phi_0 \simeq -1$ could be attributed to small flux drifts, given that the sweep is over many periods of flux for the qubit ϵ-loop.

The limits of integration fall within a unit cell of the qubit potential. The qubit eigenstates can be represented in the basis of charge states $|g\rangle = \sum_{n_1,n_2,n_4=-n_{max}}^{n_{max}} c_{n_1,n_2,n_4}|n_1,n_2,n_4\rangle$. Therefore the matrix elements of the phase operator in the qubit basis $\{|g\rangle,|e\rangle\}$ for arbitrary states $|M\rangle,|N\rangle$ look like:

$$\langle M|\hat{\varphi}_4|N\rangle = \sum_{n_1,n_2,n_4}^{n_{\max}} \sum_{n_1',n_2',n_4'}^{n_{\max}} c^*_{n_1,n_2,n_4} c_{n_1',n_2',n_4'} \left[-i\frac{(-1)^{(n_4'-n_4)}}{n_4'-n_4}\delta_{n_1,n_1'}\delta_{n_2,n_2'}\right]. \quad (13)$$

We use the representation of the phase operator in the qubit basis to obtain the different components of the qubit operator. We want only transverse coupling σ_x with matrix element $\langle 0|\hat{\varphi}_4|1\rangle \equiv \varphi_4$, and not σ_z terms that would otherwise induce dephasing in the qubit from the line. Using equation (13) we can compute the form of the operator, shown in Fig. 5

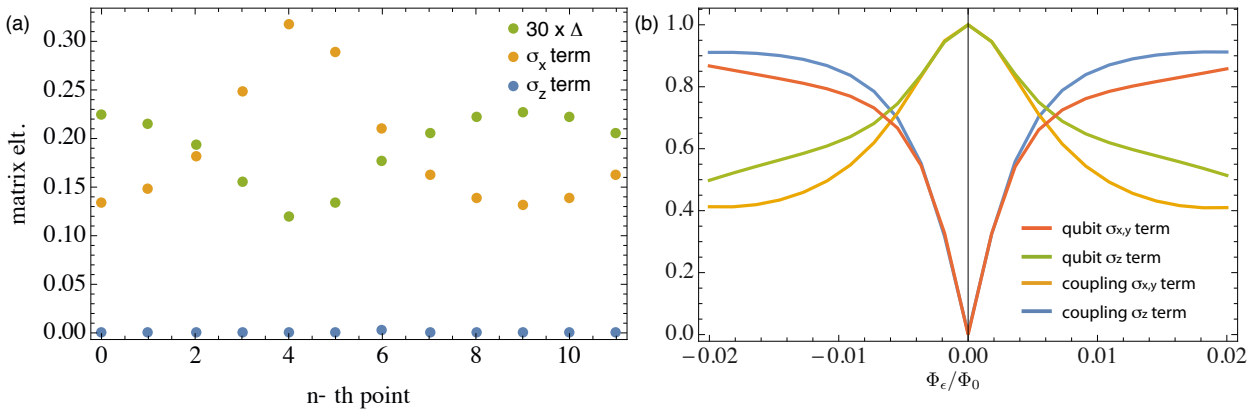

FIG. 5. (a) Calculated phase operator in the qubit basis at the symmetry point for different periods of Φ_ϵ. The operator has only σ_x component (orange) and no σ_z component (blue). The qubit splitting Δ is also plotted, its value changing approximately a factor of 2 for the parameters of the device. (b) Calculated qubit Hamiltonian terms and coupling operator terms as function of Φ_ϵ for fixed $\Phi_\beta = 0$. Away from the symmetry point the qubit Hamiltonian rotates from σ_z and starts to acquire a $\sigma_{x,y}$ component. The coupling operator follows closely the qubit Hamiltonian rotation. Therefore near the symmetry point the coupling operator rotates due to the qubit basis rotation as function of magnetic flux Φ_ϵ and not due to other terms in the Hamiltonian.

Clearly, the coupling operator only has σ_x component at the symmetry point while its magnitude increases by approximately a factor of 2.6, as expected due to the modulation of the size of the β-junction. The qubit gap is also modulated as expected due to the effective change in size of β. The change is approximately of a factor of 2. Therefore the normalized coupling $\Gamma/\Delta \sim |\varphi_\beta|^2$ (see section S7) increases by a factor of ~ 7 from $\Phi_\beta = 0$ to $\Phi_\beta = \Phi_0/2$. On Fig. 5(b) we also calculate the terms of the qubit Hamiltonian and coupling operator near $\Phi_\epsilon = \Phi_0$ for fixed $\Phi_\beta = 0$. Clearly the coupling rotates from σ_x to σ_z as the qubit Hamiltonian rotates from σ_z to σ_x. Therefore the rotation of

the coupling operator is exclusively due to the qubit Hamiltonian rotation and not from other terms. Similar rotations of the coupling operator between qubits and transmission lines or resonators were already identified in [5].

S2: SCATTERING RATES AT FINITE TEMPERATURE

Following from [6], the general definition of the master equation is

$$\dot{\rho}(t) = -\frac{i}{\hbar}[\mathcal{H}, \rho(t)] + \frac{1}{2}\sum_n [2C_n\rho(t)C_n^\dagger - \rho(t)C_n^\dagger C_n - C_n^\dagger C_n\rho(t)], \tag{14}$$

where the $C_n = \sqrt{\gamma}A_n$ are the jump operators, with γ the rate for each process with collapse operator A_n. Here $\mathcal{H}$ is the free Hamiltonian and contains the qubit part truncated to two levels, $\mathcal{H}_{\rm qb}/\hbar = \Delta\sigma_x/2 - \epsilon\sigma_z/2$ and the external driving $\mathcal{H}_d/\hbar = \Omega\sin(\omega_d t)\sigma_z$. For a qubit, the decay operator is σ_- while the excitation operator is σ_+. In terms of components, the diagonal decay terms of the master equation read

$$\dot{\rho}_{ii} = \sum_{j\neq i}(\Gamma_{ji}\rho_{jj} - \Gamma_{ij}\rho_{ii}). \tag{15}$$

Here $\Gamma_{eg} = \Gamma_1(1 + n_{\rm th})$ is the relaxation rate and $\Gamma_{ge} = n_{\rm th}\Gamma_1$ the excitation rate. $n_{\rm th}$ is the expectation value of photon number for a thermal state in equilibrium with a bath at temperature T:

$$n_{\rm th} = \frac{1}{e^{\hbar\omega/k_BT} - 1}.$$

The off-diagonal decay terms take the form (for $i \neq j$)

$$\dot{\rho}_{ij} = -\gamma_{ij}\rho_{ij}, \tag{16}$$

where the decoherence rates are $\gamma_{eg} = \Gamma_\varphi + \frac{1}{2}(\Gamma_{eg} + \Gamma_{ge}) = \Gamma_\varphi + (\Gamma_1/2)(1 + 2n_{\rm th}) \equiv \Gamma_2$, with Γ_φ the pure dephasing rate.

Explicitly, the decay equations for the four components of the density matrix now look:

$$\dot{\rho}_{ee} = \Gamma_{ge}\rho_{gg} - \Gamma_{eg}\rho_{ee} = n_{\rm th}\Gamma_1(\rho_{gg} - \rho_{ee}) - \Gamma_1\rho_{ee}, \tag{17}$$
$$\dot{\rho}_{gg} = \Gamma_{eg}\rho_{ee} - \Gamma_{ge}\rho_{gg} = n_{\rm th}\Gamma_1(\rho_{ee} - \rho_{gg}) + \Gamma_1\rho_{ee}, \tag{18}$$
$$\dot{\rho}_{eg} = -\gamma_{eg}\rho_{eg} = -[\Gamma_\varphi + \Gamma_1(1 + 2n_{\rm th})/2]\rho_{eg} = -\Gamma_2\rho_{eg}, \tag{19}$$
$$\dot{\rho}_{ge} = -\gamma_{ge}\rho_{ge} = -[\Gamma_\varphi + \Gamma_1(1 + 2n_{\rm th})/2]\rho_{ge} = -\Gamma_2\rho_{ge}. \tag{20}$$

The free evolution terms given by the commutator $[\mathcal{H}, \rho(t)]$ can be easily computed in the rotating frame of the drive frequency ω_d, under the rotating-wave approximation, where

$$\mathcal{H}/\hbar = -\delta\omega\sigma_z/2 + \Omega\sigma_x/2. \tag{21}$$

The detuning is defined as $\delta\omega = \omega_d - \omega_{\rm qb}$, $\omega_{\rm qb} = \sqrt{\Delta^2 + \epsilon^2}$ is the qubit energy splitting in units of angular frequency. ϵ is the magnetic field energy controlled by Φ_ϵ (Fig. 2(a)). The full equation of motion for all components of the density matrix are:

$$\dot{\rho}_{ee} = -\frac{i\Omega}{2}(\rho_{ge} - \rho_{eg}) + n_{\rm th}\Gamma_1(\rho_{gg} - \rho_{ee}) - \Gamma_1\rho_{ee}, \tag{22}$$
$$\dot{\rho}_{gg} = +\frac{i\Omega}{2}(\rho_{ge} - \rho_{eg}) + n_{\rm th}\Gamma_1(\rho_{ee} - \rho_{gg}) + \Gamma_1\rho_{ee} = -\dot{\rho}_{ee}, \tag{23}$$
$$\dot{\rho}_{eg} = -\frac{i\Omega}{2}(\rho_{gg} - \rho_{ee}) - i\delta\omega\rho_{eg} - \Gamma_2\rho_{eg}, \tag{24}$$
$$\dot{\rho}_{ge} = +\frac{i\Omega}{2}(\rho_{gg} - \rho_{ee}) + i\delta\omega\rho_{ge} - \Gamma_2\rho_{ge}. \tag{25}$$

Now we want to find the steady-state populations of the qubit, $\dot{\rho} = 0$. The off-resonant terms are related by

$$\rho_{eg}(i\delta\omega + \Gamma_2) = \rho_{ge}(i\delta\omega - \Gamma_2). \tag{26}$$

Adding Eqs. (22), (25),

$$\Gamma_1\rho_{ee} = -\rho_{ge}\left(\frac{i\Omega}{2}\right)\left(\frac{2\Gamma_2}{\Gamma_2 + i\delta\omega} + (\Gamma_2 - i\delta\omega)\Gamma_1 n_{\rm th}\left(\frac{2}{\Omega}\right)^2\right). \tag{27}$$

DOI: 10.1038/NPHYS3905

Using that $\mathrm{Tr}(\rho) = 1 = \rho_{ee} + \rho_{gg}$, Eq. 23 can be rewritten as

$$\rho_{ee} = \frac{1}{\Gamma_1(1+2n_{\mathrm{th}})}\left(\Gamma_1 n_{\mathrm{th}} - i\frac{\Omega}{2}(\rho_{ge} - \rho_{eg})\right). \tag{28}$$

Combining Eqs. (26)-(28) directly gives the solution for ρ_{ge}:

$$\rho_{ge} = \frac{i\Omega}{2}\frac{\Gamma_1(\Gamma_2 + i\delta\omega)}{\Gamma_2\Omega^2 + \Gamma_1(\Gamma_2^2 + \delta\omega^2)(1+2n_{\mathrm{th}})}. \tag{29}$$

Using Eq. (26) provides ρ_{eg}:

$$\rho_{eg} = -\frac{\Omega}{2\Gamma_2}\frac{i + \delta\omega/\Gamma_2}{(1+(\delta\omega/\Gamma_2)^2)(1+2n_{\mathrm{th}}) + \Omega^2/(\Gamma_1\Gamma_2)}. \tag{30}$$

Following [7], the reflection coefficient is defined as $r \equiv -i(\Gamma_1/\Omega)\langle\sigma_-\rangle$. It is easy to see that $\langle\sigma_-\rangle = \rho_{eg}$.

Therefore adding finite temperature to the system modifies the scattering parameters as follows:

$$r = r_0\frac{(-1 + i\delta\omega/\Gamma_2)}{1 + \left(\frac{\delta\omega}{\Gamma_2}\right)^2 + \frac{\Omega_R^2}{\Gamma_1\Gamma_2}}, \tag{31}$$

with $r_0 \equiv \Gamma_1/(2\Gamma_2(1+2n_{\mathrm{th}}))$ and $\Omega_R \equiv \Omega/\sqrt{1+2n_{\mathrm{th}}}$. The form of Eq. (31) is the same as the usual reflection coefficient if $n_{\mathrm{th}} = 0$. Therefore the fitted values for r_0 and Γ_2 are going to be independent of temperature, the difference will appear in Γ_1 and Γ_φ. The transmission coefficient will be given by $t = 1 + r$

$$t = 1 + r = \frac{1 + (\delta\omega/\Gamma_2)^2 + r_0(-1 + i\delta\omega/\Gamma_2) + \frac{\Omega_R^2}{\Gamma_1\Gamma_2}}{1 + (\delta\omega/\Gamma_2)^2 + \frac{\Omega_R^2}{\Gamma_1\Gamma_2}} \simeq \frac{1 + (\delta\omega/\Gamma_2)^2 + r_0(-1 + i\delta\omega/\Gamma_2)}{1 + (\delta\omega/\Gamma_2)^2}, \tag{32}$$

where the last step assumed weak driving $\Omega_R^2 \ll \Gamma_1\Gamma_2$. The resulting expression is the function used to fit the data, equation 2 in the main article. The minimum of transmission on-resonance in this case is

$$t_{\mathrm{min}} = \frac{4\Gamma_1 n_{\mathrm{th}} + 2\Gamma_\varphi(1+2n_{\mathrm{th}}) + 4\Gamma_1 n_{\mathrm{th}}^2}{(1+2n_{\mathrm{th}})(\Gamma_1 + 2\Gamma_\varphi + 2\Gamma_1 n_{\mathrm{th}})}.$$

Setting $n_{\mathrm{th}} = 0$ one restores the result of $t_{\mathrm{min}}(n_{\mathrm{th}} = 0) = \Gamma_\varphi/\Gamma_2 = \Gamma_\varphi/(\Gamma_1/2 + \Gamma_\varphi)$.

The extracted values of Γ_1 from the experiment can be then bound assuming no thermal photons (lower bound) or the maximum number of photons allowed if $\Gamma_\varphi = 0$ (upper bound), as seen in Fig. 6

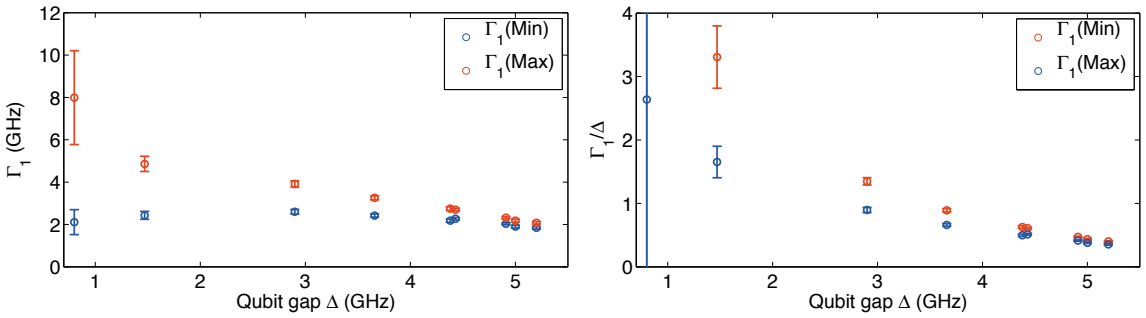

FIG. 6. (a) Γ_1 as function of qubit gap Δ, which corresponds to different coupling rates. (b) Γ_1/Δ as function of Δ.

S3: COMBINED FITTING OF RE(T) AND IM(T)

The fits in figures 2, 3 of the main text are performed simultaneously on both the real and imaginary parts. We show here the total fitted transmission components. Fig. 7 corresponds to the fits of the tunable device while Fig. 8 corresponds to the devices with fixed coupling. As explained in the main text, even though the extracted emission rates correspond to the regime where the rotating-wave approximation (RWA) is not valid, by rotating the basis of the system Hamiltonian using a polaron transformation [8] the functional form of the real and imaginary parts of the transmission follow the same analytical form as the RWA case, with a renormalized qubit splitting Δ and emission rate Γ_1 instead. Due to the fact that most data is taken below the optimal bandwidth of our amplifier and circulators below 4 GHz, the quality of the fits degrades as the system enters the regime $\Gamma_1 > \Delta$ (plots (g), (h), (i) in Fig. 7). The only relevant parameters extracted are r_0 and Γ_2. As explained in the main text, r_0 and Γ_2 are enough to set bounds on Γ_1 and the effective temperature of the system.

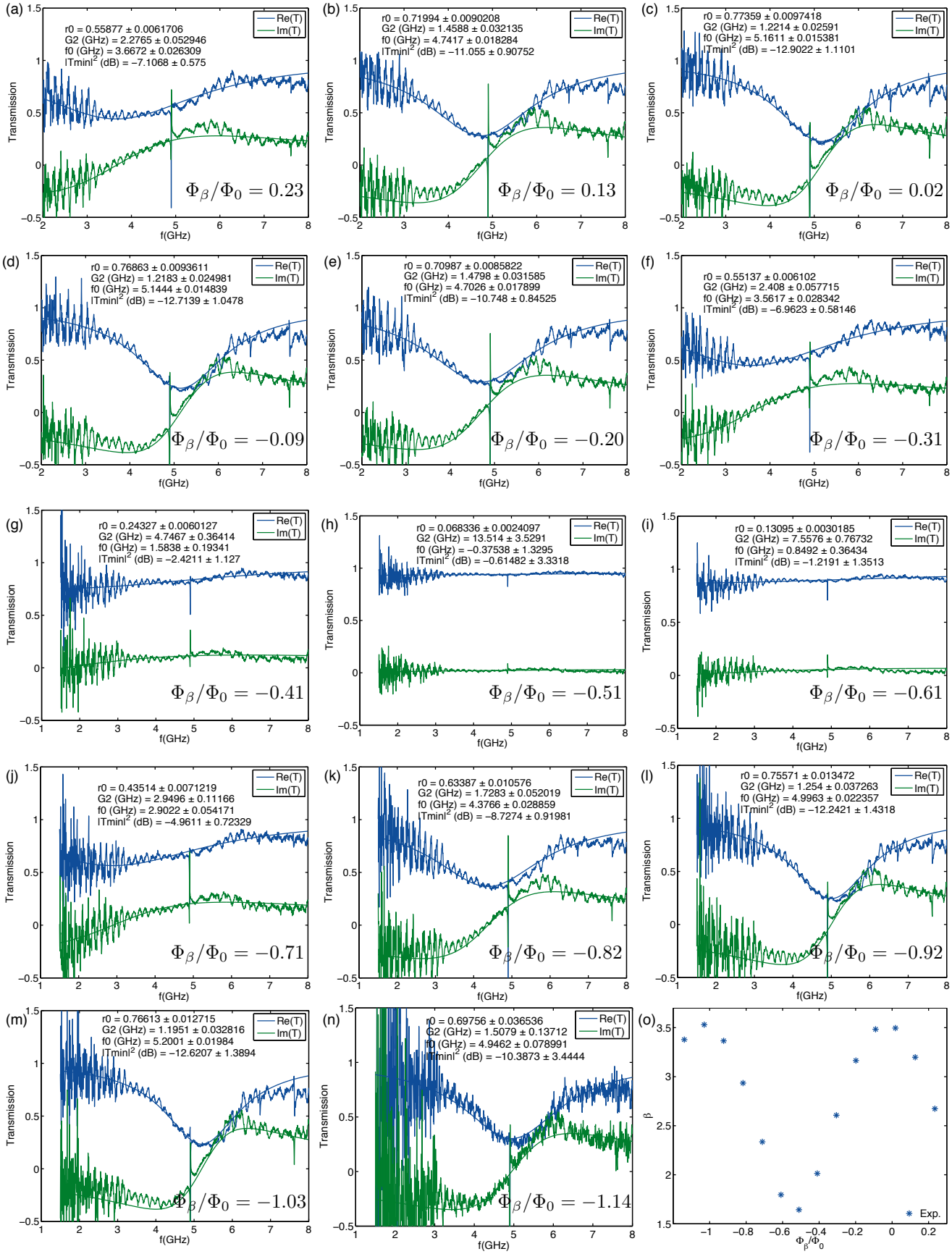

FIG. 7. (a)-(n) Combined fits corresponding to data in Fig. 3 from the main text. (o) Effective size of junction $\beta(\Phi_\beta)$.

DOI: 10.1038/NPHYS3905

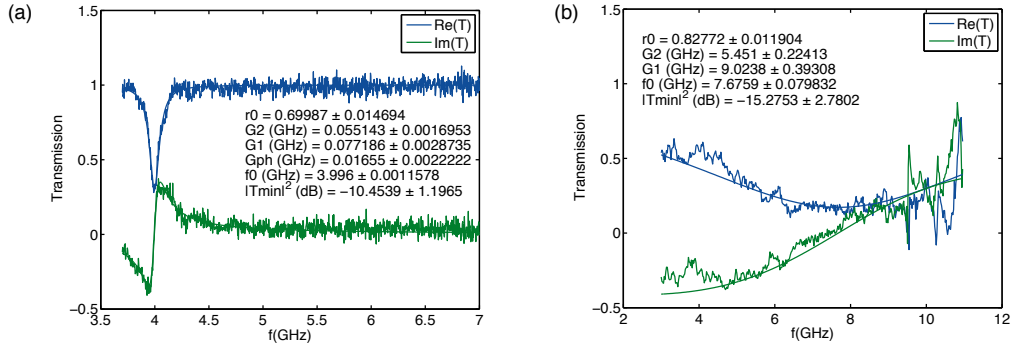

FIG. 8. Combined fits from devices with fixed coupling from Fig. 2 of the main text (a) $\beta = 3.5$, (b) β=1.8.

S4: ESTIMATES OF DEPHASING RATE

The SQUID loop in the qubit with tunable coupling may be an additional source of decoherence, especially dephasing noise since fluctuations in the flux Φ_β will directly convert into fluctuations of the qubit gap Δ. We have assumed in the main text that the enhanced linewidth of the qubit is due to thermal effects. The justification is made here where we put bounds on possible sources of dephasing.

The sensitivity of the qubit gap as function of Φ_β can be estimated by using the modulation of the qubit gap curve on Fig. 4 of the main text. An upper bound for the flux sensitivity is $\mathrm{d}\Delta/\mathrm{d}\Phi_\beta \sim 7.4\ \mathrm{GHz}/\Phi_0$. Comparing this number to the sensitivity of the qubit to flux Φ_ϵ, $\mathrm{d}\omega_{\mathrm{qb}}/\mathrm{d}\Phi_\epsilon \sim 5\ \mathrm{GHz}/(2.5\times10^{-3}\Phi_0) \sim 2\times10^3\ \mathrm{GHz}/\Phi_0$ we can see that sensitivity to flux noise in the β-loop is negligible.

Another possible source of flux noise would be through the qubit renormalization frequency as predicted by the spin-boson model. The model predicts [9] that the splitting of a two-level system in a bath of oscillators will be adiabatically renormalized to $\Delta = \Delta_0(\Delta_0/\omega_C)^{\alpha_{\mathrm{SB}}/(1-\alpha_{\mathrm{SB}})}$, where ω_C is the cutoff frequency of the environment and Δ_0 is the bare qubit gap. Since $\alpha_{\mathrm{SB}} = \Gamma_1/\pi\Delta$ (see section S6) and therefore both $\Gamma_1(\Phi_\beta), \Delta(\Phi_\beta)$ depend on Φ_β, fluctuations in Φ_β may lead to fluctuations in Δ. The sensitivity can be calculated:

$$\frac{\partial\Delta}{\partial\Phi_\beta} = \left(\frac{\Delta_0}{\omega_C}\right)^{\frac{\alpha_{\mathrm{SB}}}{1-\alpha_{\mathrm{SB}}}}\left[2\frac{\mathrm{d}\Delta_0}{\mathrm{d}\Phi_\beta} + \ln(\Delta_0/\omega_C)\frac{1}{(1-\alpha_{\mathrm{SB}})^2}\frac{\Gamma_1'\Delta_0 - \Gamma_1\Delta_0'}{\Delta_0}\right] \simeq \left(\frac{\Delta_0}{\omega_C}\right)^{\frac{\alpha_{\mathrm{SB}}}{1-\alpha_{\mathrm{SB}}}}\frac{\mathrm{d}\Delta_0}{\mathrm{d}\Phi_\beta}\left[2 + \ln(\Delta_0/\omega_C)\frac{1+\alpha_{\mathrm{SB}}}{(1-\alpha_{\mathrm{SB}})^2}\right]. \tag{33}$$

Here we used that in our experiment (Fig. 6(a)) $\Gamma_1' \equiv \mathrm{d}\Gamma_1/\mathrm{d}\Phi_\beta \approx -\Delta_0' \equiv -\mathrm{d}\Delta_0/\mathrm{d}\Phi_\beta$. The highest sensitivity occurs for $\alpha_{\mathrm{SB}} = 1/2$ where $\partial\Delta/\partial\Phi_\beta \simeq -2(\mathrm{d}\Delta_0/\mathrm{d}\Phi_\beta)$, assuming a worst case $\Delta/\omega_C \sim 1/10$. In the main text we find $\Delta/\omega_C \sim 1/15$ as the worst case. Therefore this source of dephasing is also negligible.

I. S5: TEMPERATURE SWEEPS

We want to establish more solid bounds on the maximum effective temperature $T_{\mathrm{eff}} = 90$ mK extracted from the fits of qubit spectra at different flux values, shown in Fig. 9(a), which complements the inferred n_{max} in Fig. 3(f) of the main text. Here, we study the resonance on Fig. 3(a) from the main text, where the qubit frequency is highest, as function of the base temperature of our cryostat, which is where our device is thermalized to.

In Fig. 9(b) we show the extracted maximum photon number $n_{\mathrm{max}} = (1/2)(r_0^{-1/2} - 1)$ and the corresponding effective temperature $T_{\mathrm{eff}} = (\hbar\Delta/k_B)\ln(1+n_{\mathrm{max}}^{-1})^{-1}$. Clearly T_{eff} responds at all temperatures of the cryostat. Below ~ 30 mK the effective temperature is $T_{\mathrm{eff}} = 90$ mK. Above ~ 80 mK, T_{eff} increases at the same rate as the cryostat temperature, indicating that the chip temperature is now limited by the phonon bath of the mixing chamber. The data in Fig. 9(b) support the presence of an effective bath temperature of ~ 90 mK when the cryostat is at the base temperature of $T_B = 10$ mK, as was also inferred in Fig.9(a) from the measurements of qubit spectra at different splittings. Other experiments with superconducting qubits have inferred similar effective temperatures [10]. T_{eff} is therefore a good indication of the effective system temperature and supports the observed changes in transmission for decreasing qubit splittings in Fig. 3 of the main text as having the origin in thermal effects and not dephasing.

We can also calculate the bounds on the qubit emission rate $2\Gamma_2 r_0 < \Gamma_1 < 2\Gamma_2\sqrt{r_0}$, shown in Fig. 10(a), and the normalized coupling Γ_1/Δ in Fig. 10(b). The average emission rate Γ_1 remains constant up to 100 mK, while the average normalized coupling decreases slightly for increasing temperatures.

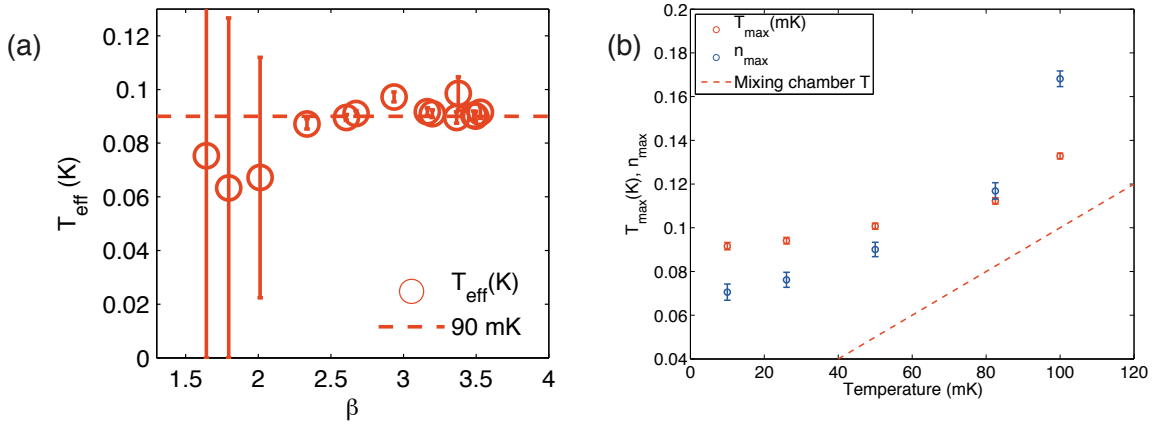

FIG. 9. (a) Calculated effective temperature from all qubit spectra in Fig. 3 of the main text. (b) Effective thermal photon number $n_{\max}$ (blue dots) and effective temperature (red dots) extracted from spectroscopy fits of qubit with tunable coupling resonances at bias flux where qubit has highest frequency $\Delta/2\pi \sim 5.2$ GHz (Fig. 3(a) main text). Above cryostat temperatures of ~ 80 mK the effective qubit temperature increases at the same rate as the cryostat. Both sets of measurements support an maximum effective temperature $T_{\rm eff}$ seen by the qubit of 90 mK.

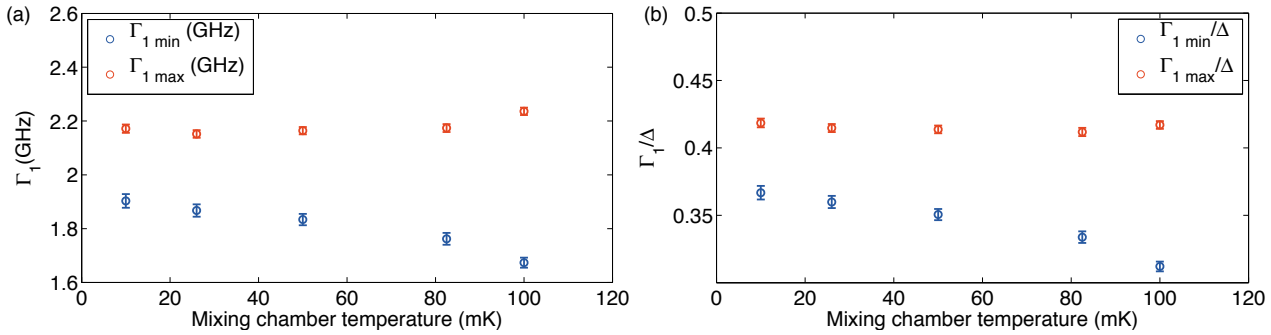

FIG. 10. (a) Calculated bounds on qubit emission rate Γ_1 as function of temperature of cryostat. The average emission rate remains constant for the temperatures used. (b) Calculated bounds on normalized coupling Γ_1/Δ of qubit to transmission line. The maximum coupling rate remains constant approximately while the average decreases.

S6: RELATION BETWEEN Γ_1 AND $\alpha_{\rm SB}$

Let us begin with the spin-boson Hamiltonian

$$H = H_0 + H_{\rm int} = \frac{\hbar\Delta}{2}\sigma_z + \sum_k \hbar\omega_k a_k^\dagger a_k + \sigma_x \sum_k g_k(a_k^\dagger + a_k), \tag{34}$$

which is characterized by the spectral function, defined as

$$J(\omega) = \frac{2\pi}{\hbar^2}\sum_k g_k^2 \delta(\omega - \omega_k) = \pi\omega\alpha_{\rm SB}, \tag{35}$$

where we have assumed an Ohmic spectral bath. As it is usual in condensed matter physics [9], [11], [12], we have expressed the spectral function $J(\omega)$ as function of a dimensionless constant $\alpha_{\rm SB}$, which characterizes the different quantum phases of the spin-boson model. More precisely, for $\alpha_{\rm SB} < 1/2$ the system is in the Markovian regime, for $1/2 < \alpha_{\rm SB} < 1$ the system is in the overdamped regime, and for $\alpha_{\rm SB} > 1$ the system is in the localized phase. Note that our definition of $J(\omega)$ differs from the one in [9] due to a factor of $1/2$ that we omit in the last term of Eq. (34).

Our aim in this section is to relate the qubit decay rate Γ_1, obtained from the master equation formalism, to the parameter $\alpha_{\rm SB}$.

To this end, we will derive a quantum master equation for the qubit. We start from the combined qubit-bath density matrix in the interaction picture

$$\rho(t) = U(t)\rho_0 U^\dagger(t), \tag{36}$$

where the unitary transformation $U(t) = \exp(iH_0 t)$ brings us into the rotating frame. This yields the following

DOI: 10.1038/NPHYS3905

time-evolution equation for the density matrix $\rho(t)$

$$\dot{\rho} = -\frac{i}{\hbar}[H_{\rm int}, \rho(t)], \tag{37}$$

being $H_{\rm int}(t)$ the coupling Hamiltonian in the interaction picture, given by

$$\begin{aligned} H_{\rm int}(t) &= U(t) H_{\rm int} U(t)^{\dagger} \\ &= (\sigma_+ e^{i\Delta t} + \sigma_- e^{-i\Delta t}) \sum_k g_k (a_k^{\dagger} e^{i\omega_k t} + a_k e^{-i\omega_k t}) \\ &= A(t) X(t), \end{aligned} \tag{38}$$

where $A(t)$, $X(t)$ are the system and bath operators, respectively.

Equation (36) can be formally integrated, yielding the following integro-differential equation

$$\dot{\rho}(t) = \rho(0) - \frac{1}{\hbar^2} \int_0^t {\rm d}\tau [H_{\rm int}(t), [H_{\rm int}(\tau), \rho_(\tau)]]. \tag{39}$$

As it is commonplace, we assume the Born approximation (weak coupling to the bath, which allows us to approximate $\rho(t) = \rho_{\rm sys}(t) \otimes \rho_{\rm b}(0)$, for any time t) and the Markov approximation (delta-correlated bath), which in turn corresponds with the Markovian dynamics of the spin-boson model defined by $\alpha_{\rm SB} < 1/2$ [8]. Under these conditions, we find a second-order differential equation for the reduced density matrix of the system

$$\dot{\rho}_{\rm sys} = -\frac{1}{\hbar^2} \int_0^t {\rm d}\tau {\rm Tr}_{\rm b} [H_{\rm int}(t), [H_{\rm int}(\tau), \rho_{\rm sys}(\tau) \otimes \rho_{\rm b}(0)]], \tag{40}$$

where ${\rm Tr}_{\rm b}(A(t)X(t))$ refers to the trace over the bath degrees of freedom $X(t)$. Expanding the double commutator, and using the cyclic property of the trace, ${\rm Tr}(AX) = {\rm Tr}(XA)$, we can rewrite the master equation as

$$\dot{\rho}_{\rm sys}(t) = \frac{\Gamma_1}{2} (2\sigma_- \rho_{\rm sys}(t) \sigma_+ - \sigma_+ \sigma_- \rho_{\rm sys}(t) - \rho_{\rm sys}(t) \sigma_+ \sigma_-), \tag{41}$$

where the spontaneous decay rate Γ_1 is given by

$$\begin{aligned} \Gamma_1 &= \frac{1}{\hbar^2} \int_{-\infty}^{\infty} {\rm d}\tau e^{-i\Delta\tau} \langle [X(\tau), X(0)]_+ \rangle \\ &= \frac{1}{\hbar^2} \int_{-\infty}^{\infty} {\rm d}\tau e^{-i\Delta\tau} \sum_k g_k^2 [(1+n_k) e^{i\omega_k \tau} + n_k e^{-i\omega_k \tau}]. \end{aligned} \tag{42}$$

In equation (43), we have introduced the symetrized bath correlation function

$$\begin{aligned} \langle [X(\tau), X(0)]_+ \rangle &= {\rm Tr}_{\rm b} [(X(\tau)X(0) + X(0)X(\tau)) \rho_{\rm b}(0)] \\ &= \sum_k g_k^2 [(1+n_k) e^{i\omega_k \tau} + n_k e^{-i\omega_k \tau}], \end{aligned} \tag{43}$$

which can be readily calculated using the bosonic commutation relations $[a_k, a_{k'}] = 0$, $[a_k, a_{k'}^{\dagger}] = \delta_{kk'}$ and the two-time correlation functions

$$\begin{aligned} \langle a^{\dagger}(t) a(t') \rangle &= \sum_k g_k^2 n_k e^{i\omega_k (t-t')}, \\ \langle a(t) a^{\dagger}(t') \rangle &= \sum_k g_k^2 (1+n_k) e^{i\omega_k (t'-t)}. \end{aligned} \tag{44}$$

In the above expressions, n_k is the average number of photons in the k-th oscillator, and is given by

$$n_k = \frac{1}{\exp(\hbar\omega_k / k_B T) - 1}. \tag{45}$$

For the sake of simplicity, but without loss of generality, we will assume that we are at zero temperature, so that $n_k = 0$. Therefore, the relaxation rate Γ_1 can be rewritten as

$$\begin{aligned} \Gamma_1 &= \frac{1}{\hbar^2} \int_{-\infty}^{\infty} {\rm d}\tau e^{-i\Delta\tau} \sum_k g_k^2 e^{i\omega_k \tau} \\ &= \frac{1}{\hbar^2} \sum_k g_k^2 \int_{-\infty}^{\infty} {\rm d}\tau e^{i(\omega_k - \Delta)\tau}. \end{aligned} \tag{46}$$

The last term in Eq. (46) is nothing but the Fourier transform of the delta function

$$\delta(\omega_k) = \frac{1}{2\pi}\int_{-\infty}^{\infty} \mathrm{d}\tau e^{i\omega_k \tau}, \tag{47}$$

yielding the following expression for Γ_1

$$\Gamma_1 = \frac{2\pi}{\hbar^2}\sum_k g_k^2 \delta(\Delta - \omega_k) = J(\Delta). \tag{48}$$

Using the second identity of Eq. (35) we finally arrive at a relation between Γ_1 and α_{SB},

$$\Gamma_1 = \pi \alpha_{\mathrm{SB}} \Delta. \tag{49}$$

It is worth mentioning that this result can be generalized for a bath at finite temperature T [11], [13], [14].

Eq. (49) is valid in the Born-Markov and rotating-wave approximations. It is known from the spin-boson model that up to $\alpha_{\mathrm{SB}} = 1/2$ (see equation 5.23 from reference [9]), corresponding to $\Gamma_1/\Delta \sim 1$ and therefore well within the ultrastrong coupling regime, Eq. (49) is still correct. The regime $0.5 < \alpha_{\mathrm{SB}} < 1$ presents more difficulties, as the spin-boson model becomes nonperturbative. Using a polaron transformation [8], an analytical model has been found [15] to yield correct results for $\alpha_{\mathrm{SB}} > 0.1$. Using this technique we calculate values for Γ_1/Δ as function of α_{SB} and compare it to equation (49), shown in Fig. 11. The results show that equation (49) is a lower bound for $\alpha_{\mathrm{SB}} > 0.1$. We assume in the analysis of our results for $\Gamma_1/\Delta > 1.5$ that equation (49) remains a lower bound.

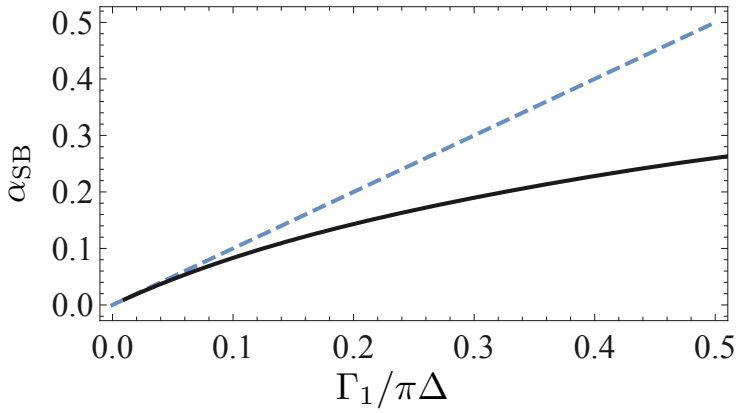

FIG. 11. Polaron ansatz [15] calculations of Γ_1/Δ as function of α_{BS} (solid-black line) compared to the Born-Markov approximation (dashed-blue line), equation (49). Clearly, equation (49) is a lower bound for $\alpha_{\mathrm{SB}} > 0.1$.

S7: THE MAXIMUM COUPLING

As detailed in [4], a flux qubit coupled to a transmission line, sharing a junction, can be calculated from the case of coupling to a single-mode resonator. We derive here the expression of the coupling rate that is used in Fig. 4(a) of the main text to fit the experimental normalized coupling rate Γ_1/Δ.

The quantized flux field in a 1D-transmission line assuming periodic boundary conditions (suitable for infinite transmission lines) takes the form

$$\hat{\phi} = \sum_k \sqrt{\frac{\hbar}{2c_0\omega_k L}}\left(\hat{a}_k e^{i(kx-\omega_k t)} + \hat{a}_k^\dagger e^{-i(kx-\omega_k t)}\right), \tag{50}$$

where the line has length L, capacitance and inductance per unit length c_0, l_0 and mode frequency ω_k. The dispersion relation is given by $\omega_k = kc = k(l_0 c_0)^{-1/2}$, c being the speed of light in the line. The coupling term takes the form (see Supplementary material in [4]):

$$\hat{H}_{\mathrm{int}} = \varphi_0 \hat{\varphi}_\beta \frac{1}{l_0}\frac{\partial \hat{\phi}}{\partial x}\delta(x), \tag{51}$$

which is nothing but the current along the transmission line times the effective node flux generated by the qubit $\varphi_0\hat{\varphi}_\beta$, with $\varphi_0 = \Phi_0/2\pi$ the reduced flux quantum and $\hat{\varphi}_\beta$ the phase operator across the qubit coupling junction β. $\delta(x)$ is

DOI: 10.1038/NPHYS3905

the Dirac delta, since the qubit is assumed to sit at the origin $x = 0$. The strength of the coupling to mode k is given by [4]

$$g_k = \frac{1}{l_0}\varphi_0\varphi_\beta\frac{1}{\sqrt{L}}\sqrt{\frac{\hbar\omega_k}{2c_0c^2}}, \tag{52}$$

with $\varphi_\beta \equiv \langle 1|\hat{\varphi}_\beta|0\rangle$ the matrix element of the phase operator across the qubit coupling junction β. The spectral density $J(\omega)$ [16], which as shown in section S6 corresponds to the spontaneous emission rate Γ_1, can be directly calculated

$$J(\omega) = 2\pi\sum_k(|g_k|/\hbar)^2\delta(\omega-\omega_k) = 2\pi\sum_k\frac{1}{l_0^2}\frac{1}{L}\frac{\omega_k}{2\hbar c_0c^2}\varphi_0^2|\varphi_\beta|^2\delta(\omega-\omega_k). \tag{53}$$

Taking the limit to the continuum, using that the density of states is $L/2\pi$,

$$J(\omega) = 2\int_0^\infty \mathrm{d}\omega_k\frac{\omega_k}{2\hbar c_0l_0^2c^3}\varphi_0^2|\varphi_\beta|^2\delta(\omega-\omega_k) = \frac{\omega}{\hbar Z_0}\varphi_0^2|\varphi_\beta|^2, \tag{54}$$

$Z_0 = (l_0/c_0)^{1/2}$ being the characteristic impedance of the transmission line. The factor of 2 in front of the integral is due to the fact that the frequency ω_k is degenerate for wavectors k and $-|k|$. By integrating over $k < 0$ and $k > 0$ we are taking into account the current fluctuations of the two semi-infinite transmission lines, which represent two independent baths. Therefore, and connecting to the traces in Fig. 4(a) of the main text, we can express the reduced coupling Γ_1/Δ as function of the expectation value of the phase operator and the impedance of the line:

$$\frac{J(\Delta)}{\Delta} = \frac{\Gamma_1}{\Delta} = \frac{1}{4e^2}\frac{\hbar}{Z_0}|\varphi_\beta|^2 = \frac{1}{2\pi}\frac{R_Q}{Z_0}|\varphi_\beta|^2, \tag{55}$$

where $R_Q = h/(2e)^2 \simeq 6.5\ \mathrm{k}\Omega$ is the resistance quantum. Equation (55) indicates that in order to increase the coupling to its highest value, Z_0 has to be as low as possible and $|\varphi_\beta|$ must be increased by making the β-junction size smaller and therefore having a phase drop of order 1 across it. Achieving $\Gamma_1/\Delta \approx 10$ is therefore within reach. From this analysis the quantity Γ_1/Δ can be understood as a normalized coupling strength.

Equation (55) has the same validity as equation (49) since it relies on equation (48). Therefore it is a lower bound for the range $0.5 < \alpha_{\mathrm{SB}} < 1$, or $1.5 < \Gamma_1/\Delta < 3$. This is verified in our experiment where in Fig. 4(a) the values of Γ_1/Δ lie above the curves for $\beta < 2$, where $\alpha_{\mathrm{SB}} > 0.5$.

BIBLIOGRAPHY

[1] A. Fedorov, P. Macha, A. K. Feofanov, C. J. P. M. Harmans, and J. E. Mooij, Phys. Rev. Lett. **106**, 170404 (2011).
[2] M. H. Devoret, *Quantum Fluctuations (Les Houches Session LXIII)* (Elsevier, 1997).
[3] J. E. Mooij, T. P. Orlando, L. Levitov, L. Tian, C. H. van der Wal, and S. Lloyd, Science **285**, 1036 (1999).
[4] B. Peropadre, D. Zueco, D. Porras, and J. J. García-Ripoll, Phys. Rev. Lett. **111**, 243602 (2013).
[5] B. Peropadre, P. Forn-Díaz, E. Solano, and J. J. García-Ripoll, Phys. Rev. Lett. **105**, 023601 (2010).
[6] B. Peropadre, J. Lindkvist, I. C. Hoi, C. M. Wilson, J. J. Garcia-Ripoll, P. Delsing, and G. Johansson, New Journal of Physics **15**, 035009 (2013).
[7] O. Astafiev, A. M. Zagoskin, A. A. Abdumalikov, Y. Pashkin, T. Yamamoto, K. Inomata, Y. Nakamura, and J. S. Tsai, Science **327**, 840 (2010).
[8] G. D. Camacho, A. Bermudez, and J. J. G. Ripoll, Phys. Rev. A **93**, 043843 (2016).
[9] A. J. Leggett, S. Chakravarty, A. T. Dorsey, M. P. A. Fisher, A. Garg, and W. Zwerger, Reviews of Modern Physics **59**, 1 (1987).
[10] J. M. Fink, L. Steffen, P. Studer, L. S. Bishop, M. Baur, R. Bianchetti, D. Bozyigit, C. Lang, S. Filipp, P. J. Leek, and A. Wallraff, Phys. Rev. Lett. **105**, 163601 (2010).
[11] U. Weiss, *Quantum Dissipative Systems*, 3rd ed. (World Scientific Publishing Company, 2008).
[12] K. Le Hur, Physical Review B **85**, 140506 (2012).
[13] C. Gardiner and P. Zoller, *Quantum Noise* (Springer-Verlag Berlin Heidelberg, 2004).
[14] A. Shnirman, Y. Makhlin, and G. Schön, Physica Scripta **2002**, 147 (2002).
[15] In preparation.
[16] A. O. Caldeira and A. J. Leggett, Annals of Physics **149**, 374 (1983).